# Thermally Bonded Nonwoven Filters Composed of Bicomponent Polypropylene/Polyester Fiber. I. Statistical Approach for Minimizing the Pore Size

**X. Y. Wang, R. H. Gong**

*Textiles and Paper, School of Materials, The University of Manchester, Manchester, United Kingdom*

Received 21 September 2005; accepted 5 December 2005
DOI 10.1002/app.23915
Published online in Wiley InterScience (www.interscience.wiley.com).

**ABSTRACT:** A statistical approach involving the uniform design of experiments and regression analysis is used to investigate the effects of thermal bonding process parameters, dwell time, thermal bonding temperature, and hot air velocity, on the pore size of three-dimensional (3D) nonwoven filters. These filters are produced from polypropylene (PP)/polyester (PET) (sheath/core) bicomponent staple fibers. The pore structures of the filter samples were examined using the capillary flow porometer. Results reveal that the statistical approach is effective in identifying the effects of the investigated process parameters on both the bubble point pore diameter and the mean flow pore diameter for the thermally bonded nonwoven filter samples. Under the optimized processing parameters for achieving the minimized pore size, the predicted minimum bubble point pore diameter is 111.12 $\mu$m and the predicted minimum mean flow pore diameter is 63.4 $\mu$m for the filter sample with the area density of 60 g/m$^2$. They are in good agreement with the experimental values of 111.71 and 60.91 $\mu$m, respectively. Microstructure features observed using scanning electron microscope indicate that the effects of the investigated process parameters on the pore size are closely related to the thermal energy delivered to the fibers and the pressure drop acting on the fabrics. © 2006 Wiley Periodicals, Inc. J Appl Polym Sci 101: 2689–2699, 2006

**Key words:** fibers; processing; structure; filtration; statistical experiment

## INTRODUCTION

Nonwoven fabrics are usually made directly from raw fiber materials in a continuous production line, thus partially or completely eliminating conventional textile operations, such as carding, roving, spinning, weaving, or knitting.[1,2] The simplicity of fabric formation, coupled with high productivity, allows nonwovens to compete favorably with wovens and knits on a performance per cost basis in many industrial applications, from simple low cost replacements for more expensive textiles to high-quality textiles. Nonwovens also provide many functions that could not be filled by traditional textiles.[1–4] However, the overwhelming majority of the research is related to the manufacture and use of nonwovens as essentially two-dimensional (2D) sheet structures. In many applications where three-dimensional (3D) fibrous web structures are needed, they have to be constructed from the flat sheet fabrics. If 3D nonwoven shell structures are produced in a single process, directly from fibers, the packaging, freight and labor costs, and the cost of wastage inevitably generated during panel cutting can be saved. This can be up to 70% of the production cost.[5] It can also shorten the process and save equipment investment, space, and energy.

To achieve uniform and isotropic properties for 3D products is much more difficult for 2D webs because the control the fiber distribution and the bonding parameters are more complex for 3D surfaces than for flat surfaces. To date, there have been only a few reports on the production of 3D nonwoven structures.[5–7] Among these, Bankert et al.[8] and Miura and Hosokawa[9] used electrophoretic deposition to fabricate 3D nonwoven shell structures. In the electrochemical process, a shaped anode and cathode were immersed in a diluted chemical binder solution containing short fibers. A DC voltage was applied between two conductive electrodes, and the fibers in the solution were deposited on the surface of the shaped anode. Then the deposited fibers were cured by heat to produce nonwoven structures with the shape of the anode. However, the nonwoven structures produced using this process were resin rich, with a resin-to-fiber ratio of 3–4 to 1. Also, the fibers used were very short, only 0.8 mm in length which can hardly be classified as textile fibers. Off et al.[10,11] patented an apparatus that adopted electrostatic field to form a nonwoven garment. During the processing, a predetermined electrostatic field is established over the garment mold

*Correspondence to:* X. Y. Wang (ljfwxy@yahoo.com).
Contract grant sponsor: The Department of Trade and Industry (UK); contract grant number: KBBB/C/012/00028.


© 2006 Wiley Periodicals, Inc.

by a matrix of conductors in the garment mold. Charged fiber layers can be deposited on the mold, followed by a thermal bonding process through an oven to form a garment. Brucciani[12] patented a process of molding thermally bonded fibrous articles. In this process, an airflow containing fibers was drawn through a perforated mold, where a fibrous web could be formed on the surface. Then hot air and cold air were applied alternatively through the web to bond and stabilize the fibers in the web. Due to the lack of fiber flow control, however, it was difficult to produce a structure with the desired fiber distribution and textile properties. Wiltshire et al.[13,14] and Thomas[15] patented a type of process to make tubular fiber performs for a fiber-reinforced plastic articles. In their process, the chopped fibers were deposited on the outside and inside surfaces of a perforated cylinder hollow tube that rotated about its axis, due to the vacuum applied from the open end of the tube. A perform can be made by spraying a resin binding. But it was a slow process for producing large, rigid shell objects with simple geometry. Eldim Applied Technologies[16] developed a process to produce 3D nonwovens, based on meltblown or spunbond technique. In this process, an airflow directed the microfibers, extruded from a spinneret, to impinge on the surfaces of 3D molds on a perforated cylinder, and then, these deposited microfibers were self bonded. Vacuum was applied inside the cylinder to help the fiber deposition and hold the web on the mold. However, demolding the web was difficult due to the continuous fiber extruding process and the intermittent motion of cylinder. Owing to the deposition of fibers on the cylinder surface, the separation among the 3D products was also a problem. Velu et al.[7] developed the Robotic Fiber Assembly and Control System (RFACS) to control meltblown-fiber deposition on a 3D mold surface to produce shaped protective garments. Apart from the high cost and complexity of the system, there is the problem that the distributions of fiber diameter are very broad, leading to unsatisfactory pore size and its distribution which are of prime importance in determining the transplant properties, the filtration efficiency, and hence, the level of protection of the nonwovens. Combined meltblowing and spunbonding processes are attractive for manufacturing of 3D shell structure nonwovens, because of the combination of the production of fibers and the production of fabrics. Some nonwoven manufacturers have been making efforts on the combined processes.[17,18] However, there are still some significant technical problems to overcome before the combined processes are applied commercially for 3D shell structure nonwovens.

Recently, a new 3D nonwoven process based on air-laying and thermal bonding has been developed.[5,6] In this process, the fabrics were directly produced from polypropylene (PP)/polyester (PET) (sheath/core) bicomponent staple fibers.

Filtration is an important part of the nonwoven industry and within the top three end-use markets for nonwoven fabrics in North America. In 2002 North American filter converters were reported to have consumed close to 1.1 billion square meters of nonwoven media, representing a market value of US $370 million.[19] The four major criteria for evaluation of filtration media are permeability, filtration efficiency, filtration capacity (or life), and filtration cost.[20] Mean flow pore diameter is a measure of the size of majority of pores and fluid permeability, and generally serves as an indicator of filtration efficiency.[21] Both the bubble point pore size and the latex bead diameter, corresponding to the filtration efficiency of 98%, are defined as the filter rating.[22,23] The bubble point pore size is often used as an important means to assure the quality of the filter media in their manufacture.[23] Permeability is another important performance of the filters, and a lower permeability of cloth leads to longer filter cycles. It is governed by the pore structures, which are normally characterized by the bubble point pore diameter, the mean flow pore diameter, and the pore size distribution.

In the present study, the pore structures of filter samples produced using the new 3D process are evaluated. In this article, the bubble point pore diameter and mean flow pore diameter of the 3D nonwoven filter samples, with respect to the three main process parameters of thermal bonding temperature, dwell time, and hot air velocity, are investigated by employing a statistical approach involving the uniform design of experiments and regression analysis. The pore structures of the 3D nonwoven filter samples were examined using the capillary flow porometer, one of the liquid extrusion techniques. Emphasis was placed on how to achieve minimized pore size by optimizing the thermal bonding process parameters. The other three structural characteristics closely related to the evaluation of filtration media, namely the fabric area density, air permeability, and the pore size distribution within the thermally bonded nonwoven filter samples will be presented in a future paper.

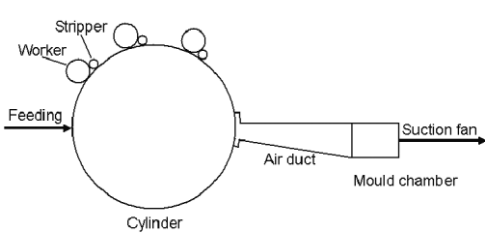


**Figure 1** The 3D web forming system.

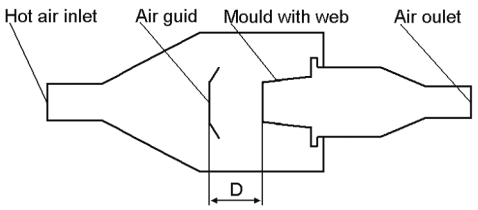


**Figure 2** The schematic diagram of web bonding.

## EXPERIMENTAL

### Preparation of nonwoven filter samples

The 3D nonwoven process includes two sections: web forming system and the bonding chamber. These are shown in Figures 1 and 2. During the processing, staple fibers are opened by an opening unit. In the present work, PP/PET (sheath/core) bicomponent staple fiber was used and its properties are listed in Table I. The opened fibers are stripped off the cylinder by high-velocity airflow and carried to the perforated 3D molds. The molds are placed on a guide track and are moved out of the mold chamber across the machine width into a bonding section for consolidation. In the bonding chamber, the hot air is drawn through the fibrous web that is supported on the original mold. The hot air inlet is connected to the hot air reservoir and the duct heater through flexible adiabatic pipes. The air outlet is connected to the suction fan. An air guide is designed to improve the flow distribution around the web. The position of the air guide can be adjusted along the central axis. Samples of the filters prepared using this process can be directly taken out of the mold chamber and their typical morphologies are shown in Figure 3.

However, to study the effects of all the different process parameters on the fabric structure of the nonwoven samples using a full factorial experimental design would be very time consuming. Instead, statistical experimental methods, such as the Taguchi and the orthogonal design methods, may be employed to reduce the number of experimental trials.[24–26] More recently, Fang and Wang[27] developed a new statistical experiment method, the uniform design of experiments. The uniform design experimental method is based on the number theory. Its aim is to replace the full spectrum of combined trials involving the experimental parameters by relatively fewer experimental trials uniformly distributed across the scope of the experimental parameters. These trials are determined by the number–theoretic method and have been mathematically proven to be a good approximation to a full spectrum of the experimental parameters. The tables for arranging various experiment trials have been listed in the reference.[25] Compared with conventional statistical methods, such as the Taguchi and orthogonal design methods, this statistical experimental method further decreases the number of trials for processes involving a large number of factors that are graded into larger numbers of factor levels.[24] Experimental results indicated that it is effective to investigate the effects of process parameters on the microstructures and properties of materials for thermal spraying and laser material processing.[26,28]

**TABLE I**
**Properties of the PP/PET (Sheath/Core) Bicomponent Fiber**

| | |
|---|---|
| Linear density (dtex) | 1.9 |
| Fibre length (mm) | 51 |
| Breaking load (gf) | 9.5 |
| Breaking elongation (%) | 40 |
| Breaking tenacity (gf/tex) | 0.5 |

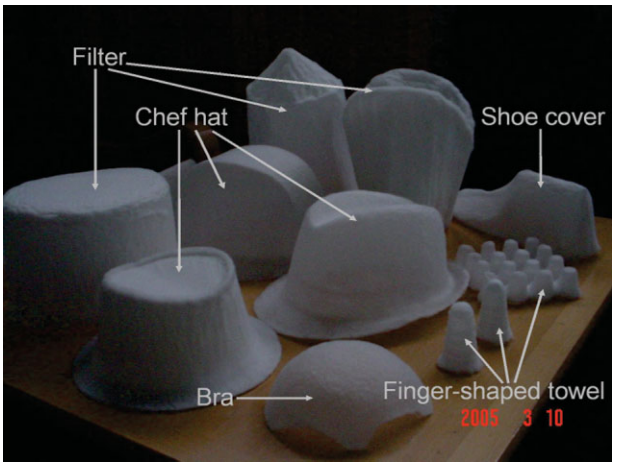


**Figure 3** Typical morphologies of the nonwoven filter samples, together with other samples, produced using the new 3D process. [Color figure can be viewed in the online issue, which is available at www.interscience.wiley.com.]

**TABLE II**
**Process Parameters Designed According to the Uniform Design Experiment Method**

| Experimental trial | Dwell time, $x_1$ (s) | Thermal bonding temperature, $x_2$ (°C) | Hot air velocity, $x_3$ (m/s) |
|---|---|---|---|
| T1 | 1 | 144 | 1.5 |
| T2 | 1 | 150 | 2.5 |
| T3 | 2 | 154 | 4 |
| T4 | 2 | 159 | 1.5 |
| T5 | 3 | 144 | 2.5 |
| T6 | 3 | 150 | 4 |
| T7 | 4 | 154 | 1.5 |
| T8 | 4 | 159 | 2.5 |
| T9 | 5 | 144 | 4 |
| T10 | 5 | 150 | 1.5 |
| T11 | 6 | 154 | 2.5 |
| T12 | 6 | 159 | 4 |

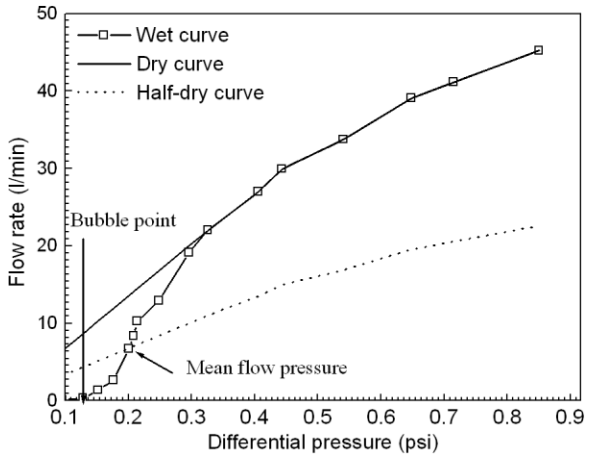


**Figure 4** Representative gas flow rates versus the differential gas pressures for one of the nonwoven filter samples.

The experimental trials for the three investigated process parameters, thermal bonding temperature, dwell time, and hot air velocity, were arranged according to Table $U_{12}$ ($6 \times 4 \times 3$) of the uniform design experiment, as listed in Table II. The design scopes of the three process parameters were determined from some preliminary experiments to ensure that the samples could be produced properly. The bonding temperature was graded into 4 levels, while the dwell time was graded into 6 levels, and the hot air velocity 3 levels. The 3 parameters were arranged into 12 experimental trials. To avoid the effect of fabric weight, all the samples were prepared with the same area density, 60 $g/m^2$.

After the bubble point pore diameter and the mean flow pore diameter of the samples are obtained, their dependences on the three investigated process parameters can be established by stepwise regression. On the basis of the regressed results, the process optimization for minimizing the pore size of the nonwoven filter can be carried out.

## Pore structure evaluation

There are mainly two techniques for evaluating the pore structures of fabrics, the mercury intrusion porosimetry and the liquid extrusion techniques.[23,29] The pressure required for the liquid extrusion techniques is generally an order of magnitude lower than that for mercury intrusion technique. Thus, the distortion of pore structure due to pressure is insignificant for the liquid extrusion techniques when compared to the mercury intrusion technique.[23,30] In addition, the liquid extrusion techniques do not involve toxic material, mercury. These make them more preferable for evaluating the pore structures of fabrics, in particular nonwovens. Liquid extrusion methods, which form the basis of ASTM method E 1294–89[31] for porosimetry of membrane filters, have been successfully used to evaluate porosity of textile materials, including nonwovens.

The pore structures were tested on a completely automated capillary flow porometer; model CFP 1500 AEX manufactured by PMI, which is capable of giving reproducible results.[32] This porometer has capability for fully automated test execution, data acquisition, data storage, and data reduction. The software is windows based. In particular, the instrument automates the saturated head gas drive technique described by Corte[33] and conforms to ASTM standard F316–03.[34]

The nonwoven filter samples were cut into circular samples of 75 mm in diameter for the tests. Prior to the tests, the samples were conditioned in the standard atmosphere for testing textiles, i.e., a relative humidity of 65% ± 2% and a temperature of 20 °C ± 2°C for 24 h.[35] After the conditioning, the samples were soaked in silicon oil, which filled the pores of the samples. The use of the silicon oil is because the fluid must have a low vapor pressure so that it will stay in the pores of the sample until pressure forces it out. It is crucial to make sure that all the pores in the sample were filled with the silicon oil that does not interact with the samples. This could be done visually by observing that all surfaces of the material were covered by a film of the wetting fluid.

Then the sample was installed into the standard-size chamber of the instrument, and fitted between two O-rings. Any gas flowing through the sample was constrained by the two O-rings to flow up and out of the top of the sample chamber. Gas flowing out the sides of the sample was trapped by the large O-ring and did not escape to the atmosphere, causing a loss in pressure and a falsely high flow rate. After starting the test, gas (air) pressure was applied on one side of the

**TABLE III**
**Results of Stepwise Regression Analysis for the Bubble Point Pore Diameter Data**

| Order | Equation | Source | Degrees of freedom | Mean square | Overall $F$ | Confidence level |
|---|---|---|---|---|---|---|
| 1 | $149.12 - 5.93x_2$ | Regression | 1 | 699.54 | 21.79 | >0.99 |
| | | Residual | 10 | 56.47 | | |
| 2 | $149.31 - 3.92 \times 10^{-2}\, x_1x_2$ | Regression | 1 | 1296.72 | 26.02 | >0.99 |
| | | Residual | 10 | 49.83 | | |

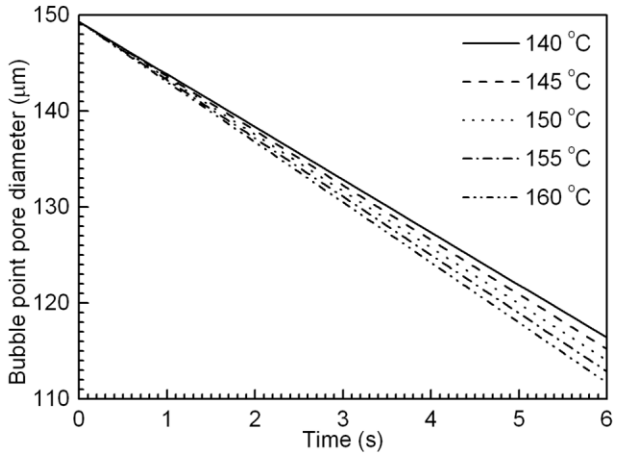


**Figure 5** Plots of the bubble point pore diameter versus the dwell time and thermal bonding temperature derived from the second-order regressed equation.

sample, which forced the liquid out of the pores. At low pressures the flow rate was zero. Flow started at a certain pressure, which was sufficient to clear some of the pores. As the pressure increased, more pores got emptied and the flow rate increased. A saturated sample will pass air when the applied pressure exceeds the capillary attraction of the fluid in the pores. Smaller pores have a higher capillary attraction, and open at higher pressures than larger pores. By comparing the gas flow rate of a wet sample and that of a corresponding dry sample at the same pressure, the percentage of flow passing through the pores larger than or equal to the specified size can be calculated from the pressure–size relationship. By increasing pressure in small steps, the flow contribution of very small pore size increments can be determined.

Figure 4 shows a representative of the recorded flow rates of dry air at a given pressure for both the wet and the dry nonwoven sample. The half-dry curve is not measured but calculated from the measured dry curve to yield half of the flow rate through dry sample at a given differential pressure. It is used to determine the mean flow pore diameter.

The pore diameter is calculated from differential pressure by applying eq. (1) to the average pressure–flow response of three repeats.[32]

$$D = 4C\gamma/P \tag{1}$$

where $D$ is the pore diameter, $\gamma$ is the surface tension of the liquid, $P$ is the differential pressure, and $C$ is a constant (2860 when $P$ is in Pa and 0.415 when $P$ is in psi).

Equation (1) shows that the differential pressure required to displace the liquid in a pore is inversely proportional to the pore diameter. Therefore, the pressure differential required to displace the liquid in a pore would be the highest at the most constricted part of the pore. Once the highest pressure is reached, the liquid from the rest of the pore will be removed, and the gas will start flowing through the pore so that the presence of the pore can be detected. Obviously, the pore diameters determined by such an extrusion flow porometry are the constricted pore diameters.

The largest pore opens up at the lowest pressure, the bubble point pressure, at which the flow starts through the wet sample. The pore diameter calculated from this pressure is the largest pore diameter or termed as the bubble point pore diameter. From the mean flow pressure, at which the amount of flow that passes through a wet sample is half the flow that passes through a dry sample, the mean flow pore diameter can be determined. Both the bubble point pore diameter and the mean flow pore diameter are important characteristics reflecting the pore size and

**TABLE IV**
**Comparison of Experimental Bubble Point Pore Diameter Data with Calculated Values using the Second-Order Regressed Equation Listed in Table III**

| Experimental trial | Experimental value ($\mu$m) | Value from the second-order regressed equation ($\mu$m) | Relative error (%) |
|---|---|---|---|
| T1 | 147.47 | 143.66 | −2.59 |
| T2 | 142.43 | 143.42 | 0.70 |
| T3 | 135.06 | 137.22 | 1.60 |
| T4 | 139.18 | 136.83 | −1.69 |
| T5 | 141.58 | 132.35 | −6.52 |
| T6 | 116.53 | 131.65 | 12.97 |
| T7 | 128.63 | 125.13 | −2.72 |
| T8 | 115.79 | 124.35 | 7.39 |
| T9 | 128.64 | 121.05 | −5.90 |
| T10 | 120.32 | 119.87 | −0.37 |
| T11 | 115.79 | 113.04 | −2.37 |
| T12 | 109.01 | 111.12 | 1.93 |

**TABLE V**
**Results of Stepwise Regression Analysis for the Mean Flow Pore Diameter Data**

| Order | Equation | Source | Degrees of freedom | Mean square | Overall $F$ | Confidence level |
|---|---|---|---|---|---|---|
| 1 | $188.18 - 0.70x_2 - 3.40x_3$ | Regression | 2 | 161.49 | 6.56 | 0.98 |
| | | Residual | 9 | 24.63 | | |
| 2 | $111.06 - 1.79 \times 10^{-1}x_2x_3 + 4.25{x_3}^2$ | Regression | 2 | 179.15 | 8.65 | >0.99 |
| | | Residual | 9 | 20.71 | | |

flow properties of a nonwoven filter sample. The bubble point pressure and the pressure at which the dry and wet curves meet yield the pore diameter range, which is another important characteristic reflecting the flow properties of the nonwoven filter sample.

### Scanning electron microscope observation

In addition, to explore why the bubble point pore diameter and the mean flow pore diameter are correlated with the investigated process parameters, the microstructure features of some representative samples were observed using the scanning electron microscope (SEM). This was carried out on an SM-300 SEM at an operative voltage of 5 kV, and the samples were covered by a layer of vacuum-sputtered Au film prior to the observation.

### Stepwise regression analysis

The correlation relationship between the bubble point pore diameter and mean flow pore diameter with the thermal bonding temperature, the dwell time, and the hot air velocity can be expressed using the following polynomial equation[36]:

$$F(x_1,x_2,x_3) = \sum_{i=1}^{3} x_i + \sum_{i=1}^{3}\sum_{i<j}^{3} x_i x_j + \ldots + \sum_{i=1}^{3}\sum_{i<j}^{3} x_i^{m-1}x_j + \sum_{i=1}^{3} x_i^m \quad (2)$$

where $F(x_1,x_2,x_3)$ is the bubble point pore diameter or the mean flow pore diameter; $x_1,x_2,x_3$ stand for the thermal bonding temperature, dwell time, and hot air velocity respectively, and $m$ is the order of the polynomial equation: a value of 1 is generally used for the simple linear regression model; a value of 2 is sometimes used for the quadratic model for better fitting of experimental data. In the present study, both 1 and 2 were used and compared.

Once the data for the bubble point pore diameter and mean flow pore diameter are obtained, the polynomial equations relating to the process parameters can be established by regression analysis. However, in eq. (2), the effects of a number of items on the bubble point pore diameter or the mean flow pore diameter are very weak and can be neglected; only those that are statistically significant to the bubble point pore diameter or the mean flow pore diameter are retained in the regressed equation.[27] The methods to sift the items include the best subset regression, the backward elimination procedure, the stepwise regression, etc.[37] In the present investigation, the stepwise regression method was used, with a self-developed program based on the Statistics Toolbox of Matlab version 6.0.0.88 (R12) on PCWIN (Mathworks).

## RESULTS AND DISCUSSION

### Regressed equations

Table III lists the results of the stepwise regression analysis in which the bubble point pore diameters from the uniform design experiment were regressed as the first- and second-order polynomial equations of the three process parameters. According to regression principles,[37,38] whether a regressed equation is statistically significant is judged from the confidence level determined from the overall Fisher value ($F$) compared to a threshold of $F$ distribution value and the regression and residual degrees of freedom, by using

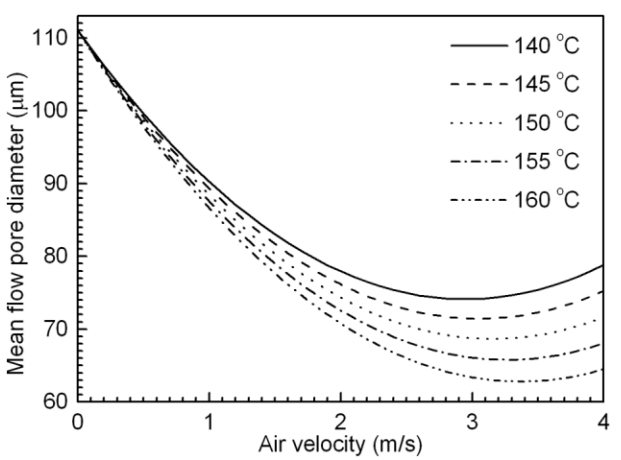


**Figure 6** Plots of the mean flow pore diameter versus the air velocity and thermal bonding temperature derived from the second-order regressed equation.

**TABLE VI**
**Comparison of Experimental Mean Flow Pore Diameter Data with Calculated Values using the Second-Order Regressed Equation Listed in Table V**

| Experimental trial | Experimental value ($\mu$m) | Value from the second-order regressed equation ($\mu$m) | Relative error (%) |
|---|---|---|---|
| T1 | 87.34 | 81.88 | −6.25 |
| T2 | 71.34 | 70.36 | −1.37 |
| T3 | 69.26 | 68.57 | −1.00 |
| T4 | 81.83 | 77.85 | −4.86 |
| T5 | 76.79 | 73.05 | −4.87 |
| T6 | 68.37 | 71.44 | 4.49 |
| T7 | 69.82 | 79.19 | 13.43 |
| T8 | 67.68 | 66.33 | −2.00 |
| T9 | 78.54 | 75.74 | −3.56 |
| T10 | 76.54 | 80.27 | 4.87 |
| T11 | 67.68 | 68.57 | 1.32 |
| T12 | 63.05 | 64.98 | 3.06 |

the $F$ test.[39] The closer to unity is the confidence level, and the more significant is the regressed equation. The precision of the prediction for the equation is determined from the residual mean square value. For example, if the process parameters are $x_1$, $x_2$, and $x_3$, there would be a probability of 0.95 that the predicted objective function (here the bubble point pore diameter and mean flow pore diameter) is within $F(x_1,x_2,x_3) \pm 2$ (residual mean square)$^{1/2}$.[39]

From Table III, it can be seen that both the first- and second-order regressed equations are statistically significant with confidence levels higher than 0.99. The second-order regressed equation has improved significance when compared with the first-order regressed equation. The first-order equation has an overall $F$ of 21.79 and prediction error of $\pm$15.03 $\mu$m. The second-order equation has an overall $F$ of 26.02 and prediction error of $\pm$14.12 $\mu$m. The first-order equation reveals that the bubble point pore diameter is significantly influenced only by the dwell time, while the second-order equations reveal that the bubble point pore diameter significantly depends on both the thermal bonding temperature and dwell time.

Figure 5 shows the plot of the bubble point pore diameter versus the thermal bonding temperature and dwell time, derived from the second regressed equation. From Table III and Figure 5, it can be deduced that within the range of the uniform design of experiments, the higher is the thermal bonding temperature and the longer is the dwell time, the smaller is the bubble point pore diameter. The minimized bubble point pore diameter, for the nonwoven fabric with area density of 60 g/m$^2$, is 113.5 and 109.17 $\mu$m for the first-order and second-order regressed equations respectively, at the thermal bonding temperature of 159°C and/or the dwell time of 6 s.

Table IV compares the experimental bubble point pore diameter data with the values calculated from the second-order regressed equations. It can be seen that they are in reasonable agreement with each other for all the experimental trials.

Similarly, from Table V, it can be seen that both the first- and second-order regressed equations for the mean flow pore diameter are statistically significant with confidence levels higher than 0.95. The second-order regressed equation has improved significance and prediction precision when compared with the first-order regressed equation. The first-order equation has a confidence level of 0.98 and prediction error of $\pm$9.93 $\mu$m. The second-order equation has a confidence level higher than 0.99, and prediction error of $\pm$9.08 $\mu$m. Both the first-order and second-order regressed equations reveal that the mean flow pore diameter mainly depends on the thermal bonding temperature and hot air velocity, while the effect of the bonding time is negligible. Figure 6 represents the plot of the mean flow pore diameter versus the thermal bonding temperature and hot air velocity derived from the second-order regressed equation.

The above results reveal that the higher is the bonding temperature, the smaller is the mean flow pore diameter. With increasing the hot air velocity, the

**TABLE VII**
**Experimental Trials for Evaluating the Validity of the Second-Order Regressed Equations**

| Experimental trial | Dwell time, $x_1$ (s) | Thermal bonding temperature, $x_2$ (°C) | Hot air velocity, $x_3$ (m/s) |
|---|---|---|---|
| VT1 | 6 | 159 | 3.4 |
| VT2 | 6 | 159 | 1.5 |
| VT3 | 3 | 150 | 2.5 |
| VT4 | 1 | 150 | 4 |
| VT5 | 1 | 144 | 1.5 |
| VT6 | 3 | 156 | 3 |

**TABLE VIII**
**Comparison of Experimental Data from Trials Listed in Table VII with Calculated Values using the Second-Order Regressed Equation Listed in Table III**

| Experimental trial | Experimental value ($\mu$m) | Value from the second-order regressed equation ($\mu$m) | Relative error (%) |
|---|---|---|---|
| VT1 | 111.71 | 111.12 | 0.53 |
| VT2 | 115.31 | 111.12 | 3.63 |
| VT3 | 129.74 | 131.67 | −1.49 |
| VT4 | 142.43 | 143.43 | −0.70 |
| VT5 | 140.89 | 143.67 | −1.97 |
| VT6 | 128.63 | 130.96 | −1.81 |

mean flow pore diameter decreases to a minimum, then increases with further increases in hot air velocity. The smallest mean flow pore diameter from the second-order regressed equation is 63.4 $\mu$m, at the thermal bonding temperature of 159°C and the hot air velocity of 3.4 m/s.

The comparison between the experimental mean flow pore diameter data with the values calculated from the second-order regressed equation is shown in Table VI. There is reasonable agreement between the predicted values and the experimental data for all the trials.

### Validity of the regressed equations

Like any other statistical experiments, the regressed equations of both the bubble point pore diameter and the mean flow pore diameter obtained from the results of the uniform design of experiments are valid only within the designed scopes of the investigated thermal bonding process parameters. To assess the validity of these equations, several experimental trials were also carried out within the design scopes of the three process parameters, as listed in Table VII. Among these experimental trials, the trial VT1 corresponds to the optimized process parameters for achieving the nonwoven filter sample with both the minimized bubble point pore diameter and the minimized mean flow pore diameter.

Tables VIII and IX compare the measured results of the trials listed in Table VII with the values predicted from the second-order regressed equations listed in Tables III and V. It can be seen that all the experimental data agree very well with those predicted from the second-order regressed equations. The experimental data falls within the intervals of the calculated value $F(x_1,x_2,x_3) \pm 2$ (residual mean square)$^{1/2}$ and have very low relative errors.

Therefore, both the second-order regressed equations are valid in predicting the bubble point pore diameter and mean flow pore diameter from the three thermal bonding process parameters. The results also justify the statistical approach used for optimizing the process parameters needed to obtain the minimal pore size when the bubble point pore diameter and the mean flow pore diameter are chosen as the objective functions.

## DISCUSSION

To explore why the bubble point pore diameter and the mean flow pore diameter are correlated with the investigated process parameters, Figures 7 and 8 present the SEM images taken from the surfaces and

**TABLE IX**
**Comparison of Experimental Data from Trials Listed in Table VII with Calculated Values from the Second-Order Regressed Equation Listed in Table V**

| Experimental trial | Experimental value ($\mu$m) | Value from the second order regressed equation ($\mu$m) | Relative error (%) |
|---|---|---|---|
| VT1 | 60.91 | 63.42 | −4.12 |
| VT2 | 76.92 | 77.93 | −1.31 |
| VT3 | 70.88 | 70.50 | 0.54 |
| VT4 | 71.34 | 71.66 | −0.45 |
| VT5 | 85.22 | 81.96 | 3.83 |
| VT6 | 69.82 | 65.54 | 6.13 |

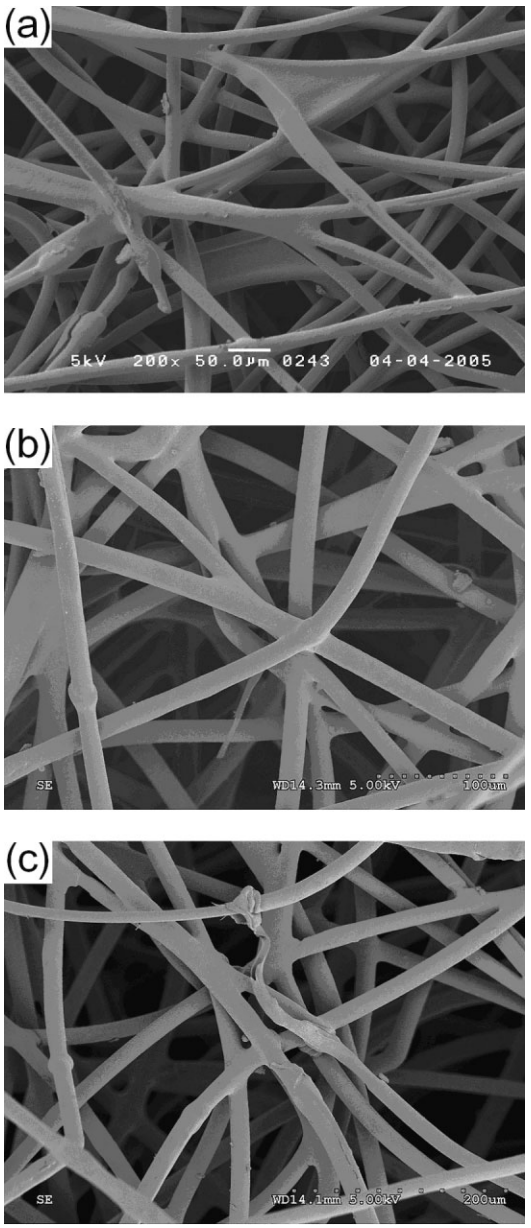


**Figure 7** SEM images taken from the surfaces of the thermally bonded nonwoven filter samples: (a) VT1, thermal bonding temperature 159°C, dwell time 6 s, and the hot air velocity 3.4 m/s; (b) VT3, thermal bonding temperature 150°C, dwell time 3 s, and the hot air velocity 2.5 m/s; (c) T6, thermal bonding temperature 150°C, dwell time 3 s, and the hot air velocity 4 m/s.

cross sections of the nonwoven samples prepared using the optimized thermal bonding process parameters and two other trials listed in Tables VII and II, respectively. These SEM images indicate that the fibers in the thermally bonded nonwoven samples are dispersed randomly to form irregularly shaped pores with a large variation in size. The higher is the thermal bonding temperature and the longer is the dwell time, the more did the PP sheath of the fibers melt during the thermal bonding process. The higher is the hot air velocity, the more compact is the fabric.

On the basis of the above SEM results, it is reasonable that the bubble point pore diameter and the mean flow pore diameter depend on the thermal bonding process parameters as expressed by the second-order regressed equations listed in Tables III and V. A higher thermal bonding temperature and a longer dwell time would tend to increases in the thermal energy delivered to the fibers from the hot air. This would increase the melting of the PP sheath of the bicomponent fiber, and hence form larger bonds

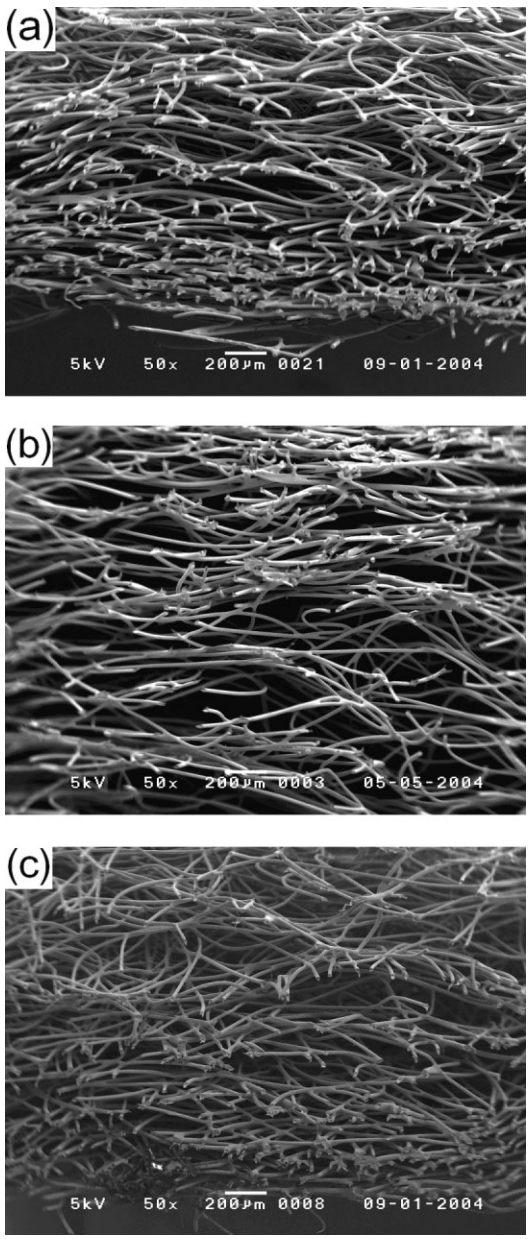


**Figure 8** SEM images taken from the cross sections of the thermally bonded nonwoven filter samples: (a) VT1, thermal bonding temperature 159°C, dwell time 6 s, and the hot air velocity 3.4 m/s; (b) VT3, thermal bonding temperature 150°C, dwell time 3 s, and the hot air velocity 2.5 m/s; (c) T6, thermal bonding temperature 150°C, dwell time 3 s, and the hot air velocity 4 m/s.

which block the passages of fluid and lead to smaller bubble point pore diameter and the smaller mean flow pore diameter. The second-order regressed equation listed in Table V and Figure 6 indicate that the mean flow bubble point pore diameter decreases to the minimum, then increases with further increase in the hot air velocity. This may be due to the fact that with increasing hot air velocity, the fabric becomes more compact due to a higher pressure drop resulting from a higher air resistance. This would cause the bubble point pore diameter and mean flow pore diameter to decrease. However, with further increasing of hot air velocity, the molten PP might be sucked away from the pores by the hot air, which would increase the opening of the fabric, and hence lead to the increased mean flow pore diameter.

It is understandable that pore size should decrease with increase in compactness of the nonwoven fabric. Figure 7 shows that the pore size is also significantly influenced by the degree of melting of the PP sheath of the bicomponent fiber. Such effect does not exist for nonwovens produced using the meltblowing and needlepunching processes. In the latter instance, different types and ratios of denier fibers may be added into the basic fibers to control the pore size for filtration applications.

## CONCLUSIONS

A statistical approach involving statistical experiment design and regression analysis has been used to optimize the thermal bonding process parameters, with emphasis on minimizing the bubble point pore diameter and the mean flow pore diameter of the thermally bonded nonwoven filter samples. The experimental bubble point pore diameters and the mean flow pore diameters were measured with the capillary flow porometer. On the basis of the obtained results, the following conclusions can be drawn:

1. The statistical approach used is valid for optimizing the thermal bonding process parameters to achieve a lower bubble point pore diameter and mean flow pore diameter for the thermally bonded nonwoven filter samples. The second-order regressed equations showed that the bubble point pore diameter mainly depends on the thermal bonding temperature and dwell time, while the mean flow pore diameter is affected by the thermal bonding temperature and hot air velocity. Within the range of used process parameters, the higher is the thermal bonding temperature and the longer is the dwell time, the smaller is the bubble point pore diameter. As for the mean flow pore diameter, the higher is the bonding temperature, the smaller is the mean flow pore diameter. Moreover, the mean flow pore diameter increases to a maximum with increasing hot air velocity, then decreases with further increasing hot air velocity.
2. On the basis of the second-order regressed equations of both the bubble point pore diameter and the mean flow pore diameter, the optimized thermal bonding processing parameters for achieving the minimized pore size are bonding temperature of 159°C, dwell time of 6 s, and hot air velocity of 3.4 m/s. The predicted minimum bubble point pore diameter is 111.12 $\mu$m and the predicted minimum mean flow pore diameter is 63.4 $\mu$m for the nonwoven sample with the area density of 60 g/m$^2$. They are in good agreement with the experimental values of 111.71 and 60.91 $\mu$m respectively.
3. Microstructure features observed using SEM indicate that the correlation between the bubble point pore diameter and the mean flow pore diameter with the thermal bonding process parameters can be explained from the effects of the process parameters on the thermal energy delivered to the fibers and the pressure drop acting on the fabrics.

## References


1. Annual Book of Standards; American Society for Testing and Materials: Philadelphia, 2002.
2. Guide to Nonwoven Fabrics, INDA: New York, 1978.
3. Malkan, S. R. In Nonwovens: Theory, Process, Performance, and Testing; Turbak, A. F., Ed.; Tappi Press: Atlanta, 1993; Chapter 1.
4. Michielsen, S.; Wang, X. Q. Int Nonwovens J 2002, 11, 35.
5. Gong, R. H.; Fang, C.; Porat, I. Int Nonwovens J 2000, 9, 20.
6. Gong, R. H.; Dong, Z.; Porat, I. Int Nonwovens J 2001, 10, 24.
7. Velu, Y.; Farer, R.; Ghosh, T.; Seyam, A. J Text Apparel Technol Manag 2000, 1, 1.
8. Bankert, R. D.; Battistelli, E. A.; Reddy, T. B. Text Res J 1973, 43, 247.
9. Miura, Y.; Hosokawa, J. Text Res J 1979, 49, 685.
10. Off, J. W. A.; Early, J. H. U.S. Pat. 4,145,388 (1979).
11. Off, J. W. A.; Early, J. H. U.S. Pat. 4,200,937 (1980).
12. Brucciani, R. L. U.K. Pat. 2,204,525 (1988).
13. Wiltshire, A. J.; Ranallo, H. U.; Czumber, F. E. U.K. Pat. 1,312,019 (1973).
14. Wiltshire, A. J. U.S. Pat. 3,687,587 (1972).
15. Thomas, C. H. U.K. Pat. 1,380,027 (1975).
16. Dong, Z. Ph.D. Dissertation, UMIST, 2002.
17. Yin, H.; Yan, Z.; Bresee, R. R. Int Nonwovens J 1999, 8, 60.
18. Yin, H.; Yan, Z.; Ko, W. C.; Bresee, R. R. Int Nonwovens J 2000, 9, 25.
19. Earley, S.; Cox, R. Filtrat Separ 2003, November, 24.
20. E. I. du Pont de nemours and Company. FiltratSepar 1998, December, 912.
21. Jena, A.; Gupta, K. Int Nonwovens J 2003, 12, 45.
22. The ASTM F 662–86: The Latex Bead Filtration Efficiency of the Flat Filter Medium.
23. Li, T. Filtrat Separ 1997, 34, 265.
24. Ying, S. Advanced Ceramics and Their Applications (in Chinese); Beijing Press of Science and Technology: Beijing, China, 1990.

25. Kingswell, R.; Scott, K. T.; Wassell, L. L. J Therm Spray Technol 1993, 2, 179.
26. Li, J. F.; Liao, H.; Ding, C. X.; Coddet, C. J Mater Process Technol 2005, 160, 34.
27. Fang K. T.; Wang, Y. Number-Theoretic Methods in Statistics; Chapman & Hall: London, 1993.
28. Li, J. F.; Li, L.; Stott, F. H. J Eur Ceram Soc 2004, 24, 3509.
29. Epps, H. H.; Leonas, K. K. Int Nonwovens J 2000, 9, 55.
30. Denbigh, K. The Principles of Chemical Equilibrium; Cambridge University Press: Cambridge, 1968.
31. ASTM Standard E1294–89: Standard Test Method for Pore Size Characteristics of Membrane Filters Using Automated Liquid Porosimeter.
32. Jena, A. K.; Gupta, K. M. J Power Sources 1999, 80, 46.
33. Sampson, W. W. J Mater Sci 2001, 36, 5131.
34. ASTM standard E F316–03: Pore Size Characteristics of Membrane Filters by Bubble Point and Mean (Middle) Flow Pore Test.
35. BS EN 20139: Textiles-Standard Atmospheres for Conditioning and Testing 1992.
36. Montgomery, D. C. Design and Analysis of Experiments; Wiley: New York, 1997.
37. Walpole, R. E.; Myers, R. H. Probability and Statistics for Engineers and Scientists, 2nd ed.; Macmillan: New York, 1978.
38. Draper, N. R.; Smith, H. Applied Regression Analysis; Wiley: New York, 1981.
39. Christensen, R. Analysis of Variance, Design and Regression; Chapman & Hall: London, 1996.